metals

MDPI

Article

Preparation and Characterization of Aminated Hydroxyethyl Cellulose-Induced Biomimetic Hydroxyapatite Coatings on the AZ31 Magnesium Alloy

Bowu Zhu [1], Yimeng Xu [1], Jing Sun [1], Lei Yang [1], Changgang Guo [1], Jun Liang [2] and Baocheng Cao [1,*]

[1] School of Stomatology, Lanzhou University, Lanzhou 730000, China; zhoubw10@lzu.edu.cn (B.Z.); xuym15@lzu.edu.cn (Y.X.); sunj15@lzu.edu.cn (J.S.); lyang15@lzu.edu.cn (L.Y.), guocg10@lzu.edu.cn (C.G.)

[2] State Key Laboratory of Solid Lubrication, Lanzhou Institute of Chemical Physics, Chinese Academy of Sciences, Lanzhou 730000, China; jliang@licp.cas.cn

* Correspondence: caobch@lzu.edu.cn; Tel.: +86-931-891-5051

Received: 13 April 2017; Accepted: 6 June 2017; Published: 8 June 2017

Abstract: The purpose of this work is to improve the cytocompatibility and corrosion resistance of magnesium alloy in the hope of preparing a biodegradable medical material. The aminated hydroxyethyl cellulose-induced biomimetic hydroxyapatite coating was successfully prepared on AZ31 magnesium alloy surface with a sol-gel spin coating method and biomimetic mineralization. Potentiodynamic polarization tests and electrochemical impedance spectroscopy showed that the hydroxyapatite/aminated hydroxyethyl cellulose (HA/AHEC) coating can greatly improve the corrosion resistance of AZ31 magnesium alloy and reduce the degradation speed in simulated body fluid (SBF). The MTT [3-(4,5-dimethylthiazol-2-yl)-2,5-Diphenyltetrazolium bromide] method and cell morphology observation results showed that the HA/AHEC coating on AZ31 magnesium alloy has excellent cytocompatibility and biological activity.

Keywords: biomaterials; corrosion; coatings; aminated hydroxyethyl cellulose; magnesium alloy; hydroxyapatite; cytotoxicity

1. Introduction

Metals and their alloys are widely used in dentistry, orthopedics and cardiovascular medicine because of their good mechanical properties and good biocompatibility as implant materials [1–4]. Magnesium is a necessary element to human nutrition, and some scholars believe that magnesium and magnesium alloys are suitable as a biodegradable implant material [5,6]. Magnesium alloys are recoverable, light, and thermally conductive. They have excellent mechanical strength and good anti-electromagnetic wave properties [7,8]. However, magnesium alloys also suffer from a low corrosion resistance in chloride solutions, and this greatly limits their applications in biomedical fields [9,10]. To guarantee the excellent mechanical properties of magnesium alloys, some scholars have performed the surface treatment of magnesium alloys by using osteo-integration or osteo-conductive performance of biomaterials to increase the corrosion resistance of magnesium alloys [11].

Hydroxyapatite has good performance in bone repair, and it is the main calcium and phosphate phase of natural bone and teeth [12,13]. Recently, thermal spraying, sputtering coating, pulsed laser deposition, sol-gel, biomimetic coating, electrophoretic deposition, and many other methods are used to prepare hydroxyapatite coatings of magnesium alloy [14–18]. Biomimetic mineralization is environmentally friendly, cheap, simple, and biocompatible, thus has attracted much attention and investigation [14]. However, direct formation of hydroxyapatite on the magnesium alloy results in

defects in mechanical and chemical stability [19]. Due to a lack of nucleation centers on hydroxyapatite growth, direct biomimetic deposition of hydroxyapatite is very difficult [20,21]. To overcome these shortcomings, a good tool is the preparation of inorganic/organic composite coatings because the organic phase in the coating can increase the stability of the inorganic phase [22,23]. Hence, organic derivatives are used to induce and promote the nucleation of hydroxyapatite and crystal process [20,21].

Cellulose is the most abundant natural polysaccharide in nature. It has many excellent features that make it helpful as a component in hybrid materials: it is a renewable homopolymer that is biodegradable, sustainable, nontoxic and highly biocompatible [24–26]. Cellulose derivatives have been described as corrosion inhibitors including carboxymethyl cellulose, hydroxypropyl cellulose, hydroxypropyl methyl cellulose, and aminated hydroxyl ethyl cellulose (AHEC) [27–31]. Sangeetha et al. shows that AHEC exhibits higher corrosion inhibition efficiency than other cellulose derivatives [31].

However, the preparation of hydroxyapatite/aminated hydroxyethyl cellulose (HA/AHEC) composite coatings on magnesium alloys is rarely reported. The purpose of this work is to study the feasibility of preparing hydroxyapatite/aminated hydroxyethyl cellulose composite coating on magnesium alloy by biomimetic mineralization and to evaluate its cytocompatibility and corrosion resistance in the hope of preparing a biodegradable medical material.

2. Materials and Methods

2.1. Materials

The AZ31 magnesium alloy was purchased from Hongxing Metal Materials Co., Ltd., Dongguan, China. Analytical grade chemical reagents were used in these experiments.

2.2. Synthesis of AHEC

The 0.5 g hydroxyl ethyl cellulose (HEC), 0.7 g (2-chloroethyl) diethylamine hydrochloride (DEH), and 0.3 g NaOH were successively added to 30 mL of deionized water. To prevent the oxidation of the HEC, 0.05 mg of sodium borohydride was added to the above solution. The reaction was completed at 50 °C for 30 min under stirring. AHEC was precipitated twice in acetone and then used in anhydrous ethanol washing after air drying [32].

2.3. Sample Preparation

The AZ31 magnesium alloy is 10 mm × 10 mm × 1 mm. The samples were mechanically polished using 600–2000 grit SiC abrasive papers. The samples were ultrasonically cleaned in 100% acetone and ethanol for 5 min each. All samples were rinsed twice by deionized water and dried in air.

2.4. Preparation of AHEC Films on AZ31 Surfaces

The sol-gel was prepared with 0.45 g AHEC dissolved in 15 mL of deionized water at 50 °C with stirring. The AHEC film was spun on the surface of the AZ31 with a spin coater (Model kw-4 desktop, Xin Youyan Electronic Technology Co., Ltd., Beijing, China). The coating solution was dripped into onto the AZ31 substrate surface, and this sample was rotated at 2000 rpm for 6 s for S1 and 5000 rpm for 12 s for S2 using a spin coater, and the operation was repeated 8 times at the same surface. After waiting for the coating film to dry in air, we used the same method to prepare the coating as on the other surface.

2.5. Preparation of HA Coating on AHEC/AZ31

The CaP solution was prepared according to Cui et al. [33]: 1.652 g $Ca(NO_3)_2$, 0.6552 g NaH_2PO_4, and 0.168 g $NaHCO_3$ were added to 500 mL demonized water. To prepare the hydroxyapatite (HA) coating, AHEC-coated AZ31 magnesium alloy was immersed in calcium phosphate solution and stored at 37 °C for 2 days. The calcium phosphate solution was replaced every 24 h. Finally, all samples

were rinsed with distilled water and dried at room temperature in air [34]. Furthermore, the bare AZ31 was directly soaked in the calcium phosphate solution with the above method to prepare HA coating on the AZ31 (HA/AZ31) as control group.

2.6. Surface Characterization

The microstructure observation, evaluation of the crystal structure, and determination of material characteristic functional groups used scanning electron microscopy (SEM, MIRA3, Tescan, Brno, Czech Republic), X-ray diffractometer (XRD, D/MAX-2400, Rigaku Co., Ltd., Tokyo, Japan) and Fourier-transform infrared (FT-IR) spectroscopy (Nicolet, Madison, WI, USA), respectively. The X-ray diffractometer used Cu-Kα radiation (λ = 1.54181 nm) at room temperature, test angle (2θ) from 20° to 80°, test voltage of 40 kV, current of 150 mA, and step size of 0.02°. The Fourier test range was 4000–500 cm^{-1} at room temperature.

2.7. Corrosion Evaluation

2.7.1. Electrochemical Measurements

The corrosion resistance of the uncoated and coated magnesium alloy was tested by common detection methods such as potentiodynamic polarization tests and electrochemical impedance spectroscopy in simulated body fluid (SBF) [35]. SBF was prepared as described by Kokubo and Takadama [36]. A three-electrode cell and electrochemical workstation was used to complete the electrochemical measurement. The working electrode, reference electrode and counter electrode were samples, Ag/AgCl electrode (saturated with KCl) and platinum plate, respectively. Before the start of the electrochemical measurement, the sample was soaked in SBF for 180 s to establish the open circuit potential. The constant scan rate was 1 mV/s, and the exposed area of samples in SBF was 0.5 cm^2. The electrochemical impedance spectrum frequency range was 0.01 to 100,000 Hz, and the results were analyzed by ZView2 software (version 2.9c, Scribner Associates, Southern Pines, NC, USA, 2005) [37]. The electrochemical measurement of each group was repeated three times to confirm the repetition rate of the result.

2.7.2. Immersion Test

To evaluate the sample's corrosion resistance, a hydrogen evolution test was done using a special device according to the description of Bakhsheshi-Rad [35]. After recording the hydrogen evolution volume of the sample, a new preparation of SBF was replaced the original solution every 24 h for a total of 7 days. Samples were repeated in triplicate.

2.8. Cell Viability Assay and Cell Morphology Examination

MC3T3-E1 cells were cultured with Dulbecco's modified Eagle's medium (DMEM) at 37 °C under an atmosphere of 5% CO_2 in a wet incubator; 10% (*v*/*v*) fetal bovine serum, 1% streptomycin and penicillin was added to DMEM. The extraction media was prepared using DMEM and an extracting ratio of 1 cm^2/mL [34]. Cells were cultured (10^4 cells per well) in the 96-well plates for 24 h. The MC3T3-E1 cells were cultured in the DMEM as the negative group. DMEM was then replaced with extraction medium. The MTT [3-(4,5-dimethylthiazol-2-yl)-2,5-Diphenyltetrazolium bromide] method was used after 1, 4 and 7 days of culture. This experiment was independently repeated three times. The proliferation rate of MC3T3-E1 cell was determined with MTT method. The absorbance at 570 nm was then recorded with a microplate reader (Elx 800, Bio-Tek, Winooski, VT, USA), and the data were also subjected to unpaired single tailed Student's *t*-test. A value of $p < 0.05$ was considered as significant. We also used an inverted optical microscope (IX2-Olympus, Tokyo, Japan) to obtain cell culture photos.

3. Results and Discussion

3.1. Characterization of the Samples Surfaces

Figure 1 shows the surface morphology of AZ31 (Figure 1a), the AHEC (Figure 1b) and HA/AHEC (Figure 1c) coated substrates. It is clear that the surface morphology of AHEC coated AZ31 is a uniform and dense structure compared with the untreated of AZ31. Scratches are not observed in AHEC/AZ31 surface, which contrasts Fragal's result [38]. The surface of the HA/AHEC-coated AZ31 samples is flower-like and homogeneous. It is composed of porous and consistent flake-like crystals. The porous structure is good for the promotion of bone cell biology reaction such as induction of bone apatite formation, which stimulates the osteoblast proliferation [39]. According to the Laurencin et al. [39], the porous structure may be caused by hydrogen release. The surface morphologies of AZ31, AHEC/AZ31, and HA/AHEC/AZ31 samples after immersion in SBF for 7 days are shown in Figure 1d–f. The surface of uncoated AZ31 samples has many wide and deep cracks and pits, but with little HA. On the AHEC coating, the cracks and pits become smaller with many dense and spherical HA particles. This may be the AHEC inducing HA formation in SBF [38]. However, the surface of HA/AHEC/AZ31 shows the fewest cracks and pits with a more narrow and shallow structure. These cracks are caused by water loss of the corrosion products and surface shrinkage [40]. Thus, we infer that HA/AHEC double coating can promote the corrosion resistance of AZ31 and protect AZ31 from SBF corrosion. The cross-section morphologies of the HA, AHEC, and HA/AHEC coating are presented in Figure 1g–i. No obvious dividing line is seen in the HA/AHEC-coated AZ31. Thus, we infer that the AHEC coating could induce the formation of HA coating on the AZ31 magnesium alloy surface.

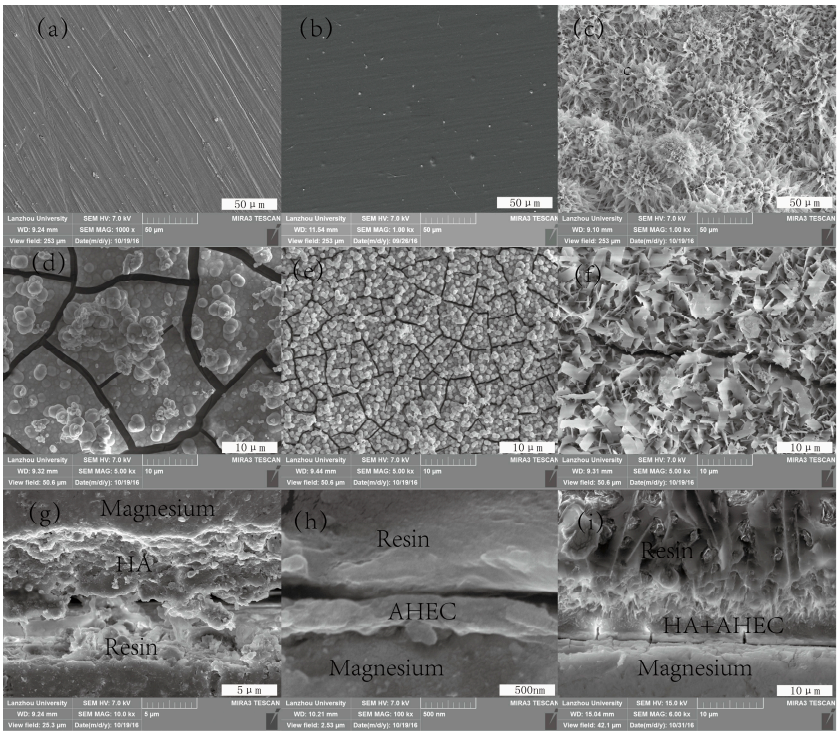

Figure 1. Scanning electron microscopy (SEM) images of AZ31, aminated hydroxyethyl cellulose (AHEC)/AZ31, and hydroxyapatite/aminated hydroxyethyl cellulose (HA/AHEC)/AZ31 specimens: before (**a**–**c**); and after (**d**–**f**) immersion in simulated body fluid (SBF) for 7 days; and the cross-sections of: (**g**) HA/AZ31; (**h**) AHEC/AZ31; and (**i**) HA/AHEC/AZ31.

XRD patterns of all specimens are shown in Figure 2. Except for the characteristic peak of magnesium alloy on AZ31 substrate, the peaks of magnesium hydroxide is also detected at $2\theta = 58°$.

This may be due to the formation of $Mg(OH)_2$ in the polishing process. Compared to the uncoated AZ31, the AHEC coating of AZ31 shows no obvious differences. This may be because the AHEC film is relatively thin with amorphous crystallinity [41]. However, in addition to the characteristic peak of magnesium alloy, the HA/AHEC/AZ31 produces a new sharp and narrow characteristic peak. The new peaks are located at 2θ = 25.9°, 32°, 32.6° and 54° from the (002), (211), (300) and (002) reflection of HA, respectively [34,42]. However, compared with the pure HA, some peaks of HA are not observed in the HA/AHEC/AZ31. These results show that the coating on the AHEC/AZ31 surface might be Ca-deficient HA [43,44].

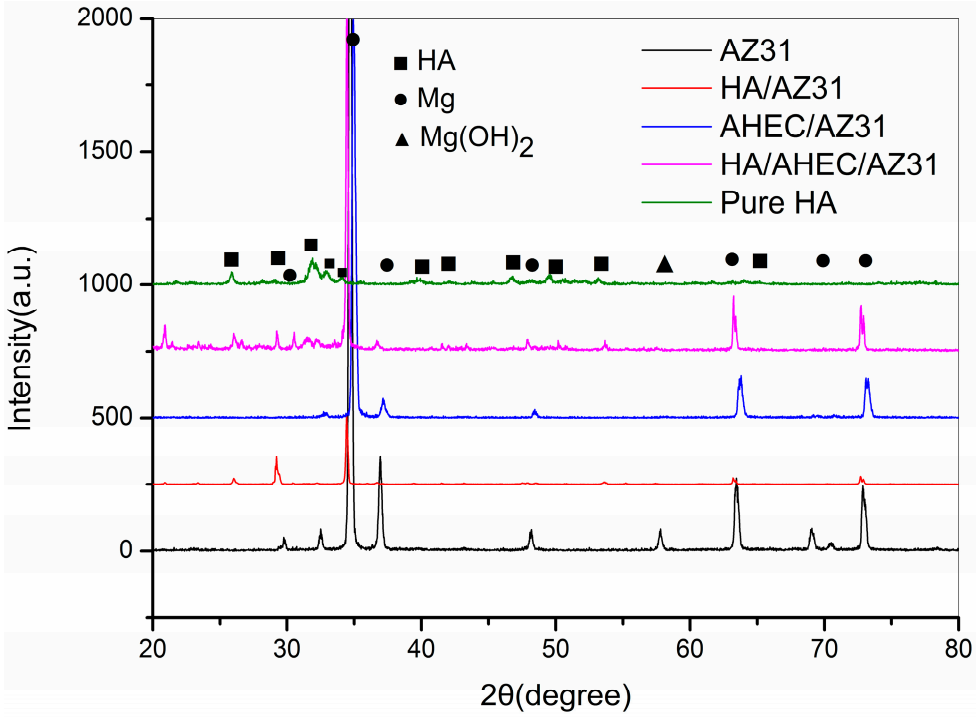

Figure 2. X-ray diffractometer (XRD) pattern of AZ31, HA/AZ31, AHEC/AZ31, HA/AHEC/AZ31, and Pure HA specimens.

The FT-IR spectra of AZ31, AHEC, AHEC/AZ31, HA/AHEC/AZ31, and pure HA are presented in Figure 3. The spectrum of AHEC has a broad peak at 3417 cm^{-1} indicating hydroxyl groups. The bands at 1370, 1409 and 1456 cm^{-1} represent the –CH, $–CH_2$ and $–CH_3$ groups of AHEC, respectively [32]. The amino peak at 2847 cm^{-1} is small [32]. These results confirm that we successfully synthesize AHEC. In the spectrum of AHEC coated on AZ31, the characteristic band of AHEC is consistent with the synthesis of AHEC. Thus, the hydroxyl and amine groups are involved in the adsorption of AHEC on AZ31. The HA/AHEC/AZ31 samples have a broad peak for the hydroxyl group at 3500 cm^{-1}. Compared to other groups, new sharp peaks are seen at 1094, 604 and 566 cm^{-1}. This may be due to the phosphate groups [33]. Additionally, the peaks of HA/AHEC/AZ31 are consistent with the pure HA. These results indicate that hydroxyapatite is successfully prepared on the surface of AHEC/AZ31. However, we also see the existence of carbonate bands (CO_3^{2-}) at 1658 cm^{-1}, and this may be attributed to small amounts of carbonate groups in hydroxyapatite [34].

The material characterization results confirm the hydroxyapatite coating is formed on the AZ31 magnesium alloy. Some scholars [38,45] suggest that the formation is due to the hydroxyl groups of AHEC adsorbing Ca^{2+} in solution. This forms positively charged groups of the surface. Thus, many negatively charged groups in the solution combine with calcium ions such as OH^-, PO_4^{3-}, etc. As a result, the AZ31 magnesium alloy surface forms the hydroxyapatite coating.

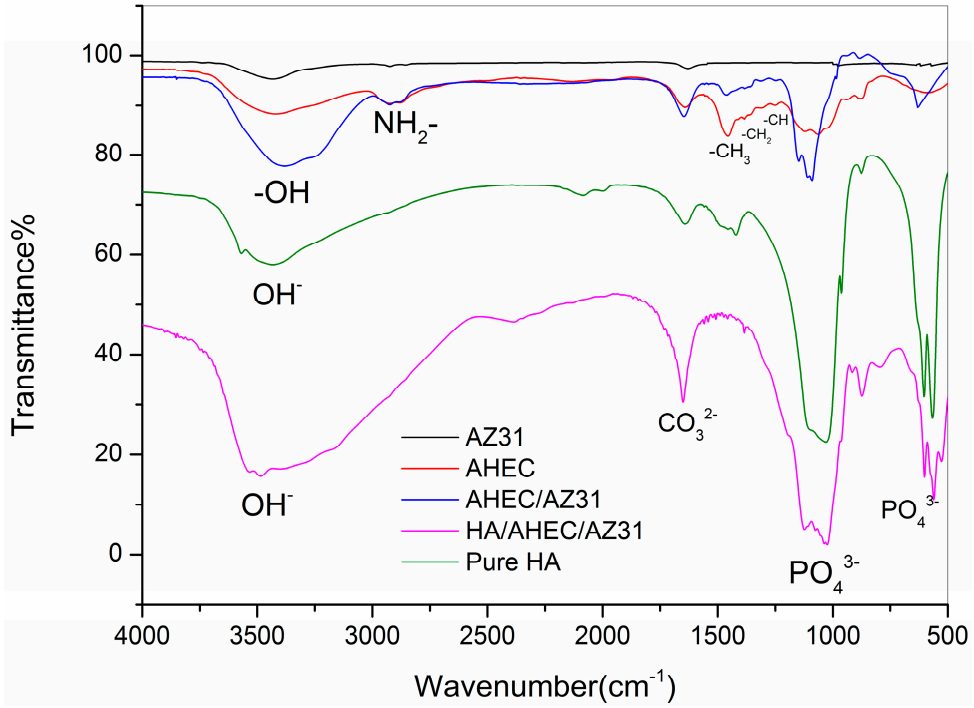

Figure 3. Fourier-transform infrared (FT-IR) spectrum of AZ31, AHEC, AHEC/AZ31, HA/AHEC/AZ31, and Pure HA.

3.2. Corrosion Resistance Analysis

3.2.1. Polarization Studies

The potentiodynamic polarization curves for AZ31, HA/AZ31, AHEC/AZ31, and HA/AHEC/AZ31 in SBF at room temperature are displayed in Figure 4, and the relative electrochemical parameters are listed as the inset. The corrosion potential (Ecorr) of HA/AHEC/AZ31 is −1.229 V, which is higher than that of bare AZ31 (−1.414 V), HA/AZ31 (−1.391 V) and AHEC/AZ31 (−1.316 V). In addition, the corresponding corrosion densities (Icorr) from Tafel fitting are 2.09×10^{-7}, 2.23×10^{-6}, 3.93×10^{-6} and 7.09×10^{-7} A/cm^2 for HA/AHEC/AZ31, AZ31, HA/AZ31, and AHEC/AZ31, respectively. Compared to bare AZ31, the Ecorr for HA/AHEC/AZ31 increases about 185 mV, and the Icorr value reduces 10 times. This shows that the HA/AHEC coating significantly promotes corrosion resistance of AZ31. The corrosion rate is decreased, and this decreases the corrosion ion concentration of direct contact with the surface of the AZ31 substrate [31].

3.2.2. EIS Test

Electrochemical impedance is a perturbative signal technology and slight damage on the surface of the sample [35]. Figure 5a is a Nyquist curve of bare AZ31, AHEC and HA/AHEC coated samples soaked in SBF solution with a fitting curve for all groups. It is clear that both uncoated and coated samples are only a capacitive reactance arc at high frequency area. A significantly larger diameter is observed on coated samples than the AZ31 substrate. Hu et al. showed a capacitive reactance arc of coated specimens showed that the electrochemical reaction area of coating and metal interface is small during soaking [46]. The electrochemical impedance spectroscopy (EIS) of AZ31 and coated substrates are fitted using the equivalent circuit of Model A and Model B in Figure 5, respectively. In this circuit, Rs, C1, R1 and R2 represent the solution resistance, the coating capacitance, the coating pore resistance and the charge transfer resistance, respectively. Generally speaking, a good impedance sample can show a high charge transfer resistance. The charge transfer values are 5855 Ω cm^2, 3281 Ω cm^2 and 1259 Ω cm^2 for HA/AHEC/AZ31, AHEC/AZ31, and AZ31, respectively. It is obvious that the charge

transfer impedance of HA/AHEC/AZ31 is biggest, and this shows that the HA/AHEC coating can significantly improve corrosion resistance of AZ31 by preventing corrosion ions direct contact with the substrate [47].

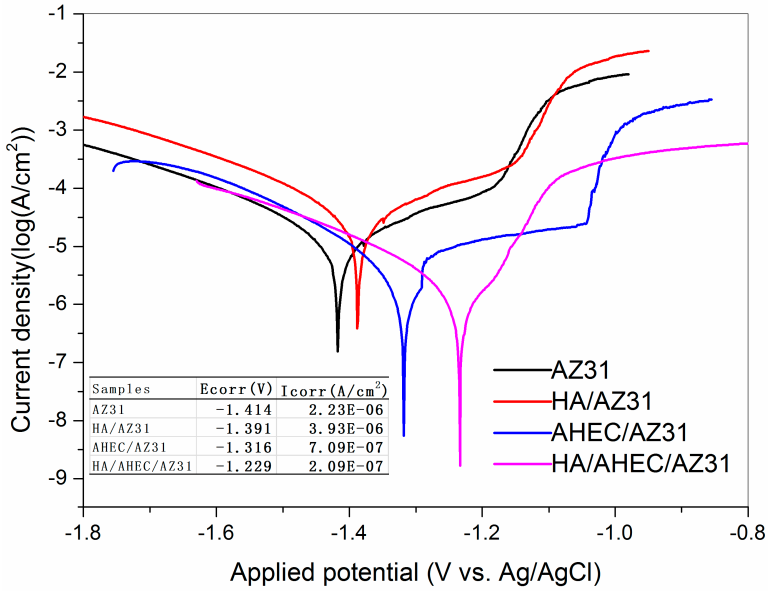

Figure 4. The potentiodynamic polarization curves for AZ31, HA/AZ31, AHEC/AZ31, and HA/AHEC/AZ31 in SBF at room temperature; the relative electrochemical parameters are listed in the inset.

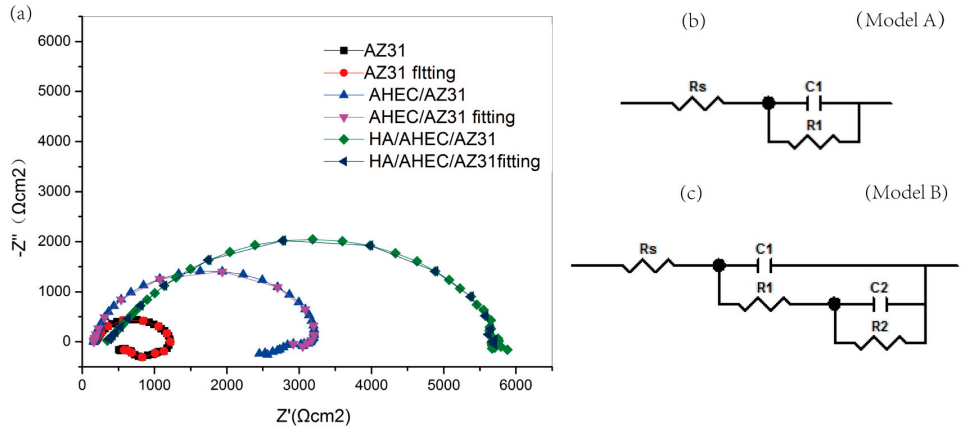

Figure 5. (**a**) Nyquist curve; and (**b**,**c**) the equivalent circuit of all samples soaked in SBF.

3.2.3. Immersion Test Studies

The line chart of cumulative hydrogen gas for the uncoated and coated samples in the SBF for seven days are shown in Figure 6. The mean hydrogen evolution rate of HA/AHEC/AZ31, AHEC/AZ31, HA/AZ31, and AZ31 are 0.31, 0.44, 0.64, and 0.92 mL/cm^2/day, respectively. Compared to other groups, the average hydrogen release rate of the HA/AHEC-coated sample is the smallest, and this indicates that the coating can effectively reduce the degradation rate of AZ31 in SBF. Thus, the HA/AHEC coating can significantly improve the corrosion resistance of the AZ31 substrate. This acts as a protection layer.

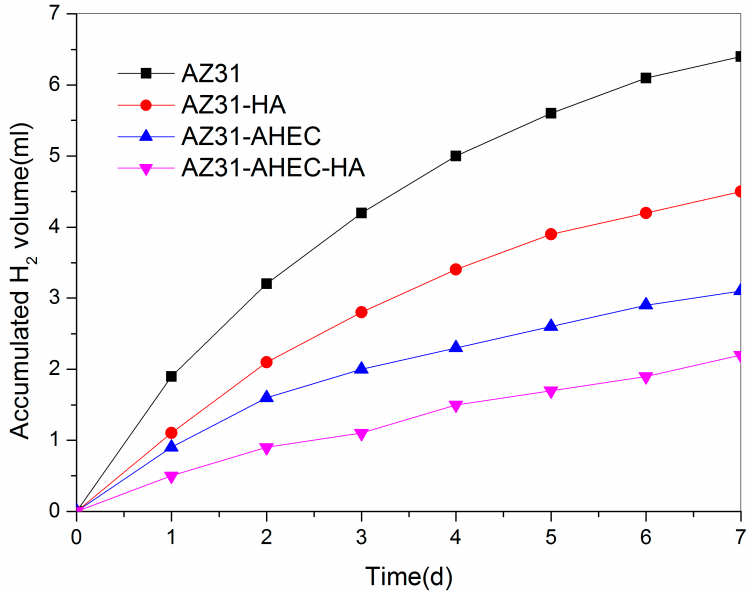

Figure 6. The line chart of cumulative hydrogen gas for the uncoated and coated samples in SBF for seven days.

3.3. Cytotoxicity Evaluation

Cell proliferation is measured with the MTT assay and MC3T3-E1 cells. Cell morphology observations evaluate the cytotoxicity of all samples. The cell viability values of AZ31, HA/AZ31, AHEC/AZ31, and HA/AHEC/AZ31 specimens are displayed in Figure 7. The cell proliferation rate of all leaching solution cultured cells is higher than 80% for one, four and seven days, which shows that none of the samples have cytotoxicity—they are non-toxic. We conclude that all samples possess good cytocompatibility. In addition, the cell proliferation rate of HA/AHEC-coated AZ31 for different period is the highest, and it is more than the negative control group ($p < 0.05$). It can be concluded that the HA/AHEC coating is a bioactive film, which can apparently promote the proliferation of MC3T3-E1 cells. It may be that the hydroxyapatite dissolved liquid has acceleration for MC3T3-E1cell proliferation and differentiation [38].

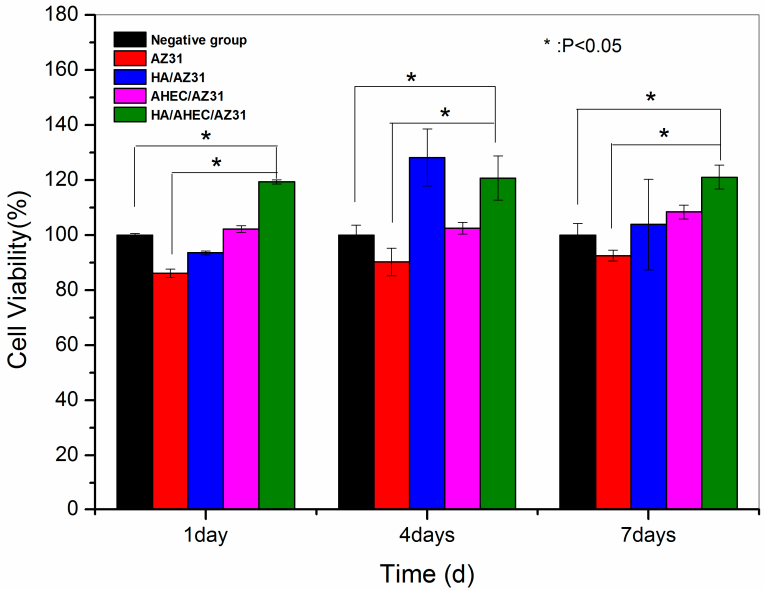

Figure 7. The cell viability of AZ31, HA/AZ31, AHEC/AZ31, and HA/AHEC/AZ31 specimens.

Inverted microscope images (20×) for the MC3T3-E1 cells cultured with extracts originated from AZ31 (Figure 8a), AHEC/AZ31 (Figure 8b), and HA/AHEC/AZ31 (Figure 8c) specimens, and the negative control group (Figure 8d) for 7d are presented in Figure 8. The cell number increased in the coating group relative to the negative control group. In addition, the cell number of the HA/AHEC coating is the highest. The cell morphology is generally similar across samples, but the HA/AHEC coating group is more regular, consistent, and closer to the negative control group. These data suggest that the HA/AHEC-coated AZ31 has good cytocompatibility.

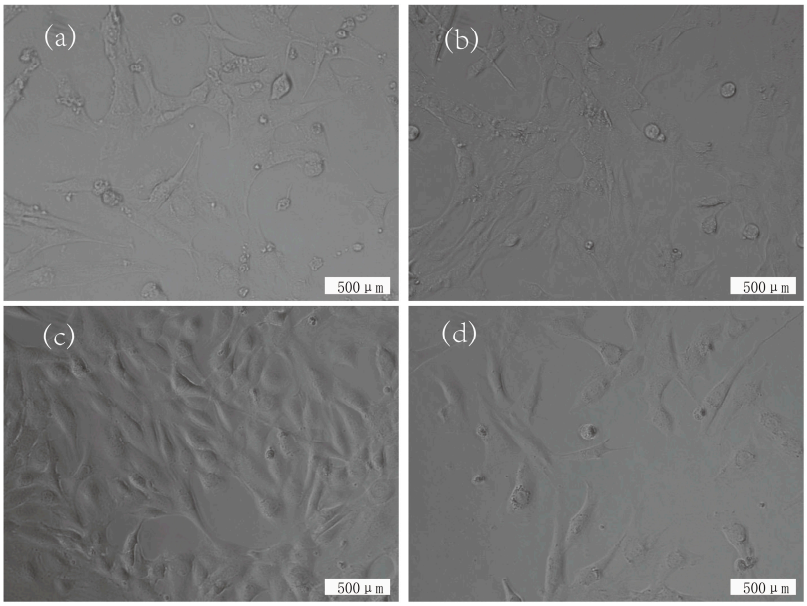

Figure 8. Inverted microscope images (20×) for the MC3T3-E1 cells cultured with extracts originating from: AZ31 (**a**); AHEC/AZ31 (**b**); and HA/AHEC/AZ31 (**c**) specimens; and the negative control group (**d**) for 7d.

4. Conclusions

A homogeneous HA/AHEC double coating with AHEC as the nucleation center is successfully prepared on AZ31 magnesium alloy surface using a sol-gel spin coating method and biomimetic mineralization. Corrosion resistance analysis shows that the HA/AHEC coating could greatly improve the corrosion resistance of AZ31 magnesium alloy and reduce the degradation speed in simulated body fluid. In vitro cytotoxicity evaluation results show that the HA/AHEC double coating composite material has not cytotoxic reaction to MC3T3-E1 cells and significantly enhances the cellular responses. Finally, these results suggest that the good corrosion resistance and cytocompatibility of HA/AHEC composite-coated AZ31 magnesium alloy has potential utility as a medical implant material.

Acknowledgments: This work was funded by the Natural Foundation of Gansu Province, China (grant No. 1208RJZA236) and the Key Technology Support Program of Gansu Province, China (grant Nos. 1604FKCA089 and 1504FKCA095). We sincerely thank Zhenjun Peng from the State Key Laboratory of Solid Lubrication, Lanzhou Institute of Chemical Physics, Chinese Academy of Sciences for the technical assistance during these studies. We also appreciate the valuable comments provided by other members of our laboratories. We thank LetPub (www.letpub.com) for its linguistic assistance during the preparation of this manuscript.

Author Contributions: Bowu Zhu and Baocheng Cao conceived and designed the experiments; Bowu Zhu and Yimeng Xu performed the experiments; Bowu Zhu, Jing Sun, Lei Yang and Changgang Guo analyzed and discussed the data; Bowu Zhu wrote the paper; and Jun Liang and Baocheng Cao did the revision and direction of the work.

Conflicts of Interest: The authors declare no conflict of interest.

References

1. O'Brien, B.; Carroll, W. The evolution of cardiovascular stent materials and surfaces in response to clinical drivers: A review. *Acta Biomater.* **2009**, *5*, 945–958. [CrossRef] [PubMed]
2. Sydow-Plum, G.; Tabrizian, M. Review of stent coating strategies: Clinical insights. *Mater. Sci. Technol.* **2013**, *24*, 1127–1143. [CrossRef]
3. Raman, V.; Tamilselvi, S.; Rajendran, N. Electrochemical impedance spectroscopic characterization of titanium during alkali treatment and apatite growth in simulated body fluid. *Electrochim. Acta* **2007**, *52*, 7418–7424. [CrossRef]
4. Srinivasan, A.; Ranjani, P.; Rajendran, N. Electrochemical polymerization of pyrrole over AZ31 Mg alloy for biomedical applications. *Electrochim. Acta* **2013**, *88*, 310–321. [CrossRef]
5. Song, G.; Song, S. A possible biodegradable magnesium implant material. *Adv. Eng. Mater.* **2007**, *9*, 298–302. [CrossRef]
6. Witte, F.; Hort, N.; Vogt, C.; Cohen, S.; Kainer, K.U.; Willumeit, R.; Feyerabend, F. Degradable biomaterials based on magnesium corrosion. *Curr. Opin. Solid State Mater. Sci.* **2008**, *12*, 63–72. [CrossRef]
7. Gray, J.E.; Luan, B. Protective coatings on magnesium and its alloys—A critical review. *J. Alloy Compd.* **2002**, *336*, 88–113. [CrossRef]
8. Kojima, Y. Project of platform science and technology for advanced magnesium alloys. *Mater. Trans.* **2001**, *42*, 1154–1159. [CrossRef]
9. Wang, L.; Zhang, K.; Sun, W.; Wu, T.; He, H.; Liu, G. Hydrothermal synthesis of corrosion resistant hydrotalcite conversion coating on AZ91D alloy. *Mater. Lett.* **2013**, *106*, 111–114. [CrossRef]
10. Feng, J.; Chen, Y.; Liu, X.; Liu, T.; Zou, L.; Wang, Y.; Ren, Y.; Fan, Z.; Lv, Y.; Zhang, M. In-situ hydrothermal crystallization $Mg(OH)_2$ films on magnesium alloy AZ91 and their corrosion resistance properties. *Mater. Chem. Phys.* **2013**, *143*, 322–329. [CrossRef]
11. Gopi, D.; Prakash, V.C.A.; Kavitha, L.; Kannan, S.; Bhalaji, P.R.; Shinyjoy, E.; Ferreira, J.M.F. A facile electrodeposition of hydroxyapatite onto borate passivated surgical grade stainless steel. *Corros. Sci.* **2011**, *53*, 2328–2334. [CrossRef]
12. Kumar, A.; Negi, Y.S.; Choudhary, V.; Bhardwaj, N.K. Microstructural and mechanical properties of porous biocomposite scaffolds based on polyvinyl alcohol, nano-hydroxyapatite and cellulose nanocrystals. *Cellulose* **2014**, *21*, 3409–3426. [CrossRef]
13. Tadic, D.; Peters, F.; Epple, M. Continuous synthesis of amorphous carbonated apatites. *Biomaterials* **2002**, *23*, 2553–2559. [CrossRef]
14. Yang, Y.; Kim, K.H.; Ong, J.L. A review on calcium phosphate coatings produced using a sputtering process—An alternative to plasma spraying. *Biomaterials* **2005**, *26*, 327–337. [CrossRef] [PubMed]
15. Gyorgy, E.; Grigorescu, S.; Socol, G.; Mihailescu, I.N.; Janackovic, D.; Dindune, A.; Kanepe, Z.; Palcevskis, E.; Zdrentu, E.L.; Petrescu, S.M. Bioactive glass and hydroxyapatite thin films obtained by pulsed laser deposition. *Appl. Surf. Sci.* **2007**, *253*, 7981–7986. [CrossRef]
16. Oliveira, A.L.; Reis, R.L.; Li, P. Strontium-substituted apatite coating grown on Ti6Al4V substrate through biomimetic synthesis. *J. Biomed. Mater. Res. Part B* **2007**, *83*, 258–265. [CrossRef] [PubMed]
17. Kawashita, M.; Itoh, S.; Miyamoto, K.; Takaoka, G.H. Apatite formation on titanium substrates by electrochemical deposition in metastable calcium phosphate solution. *J. Mater. Sci. Mater. Med.* **2008**, *19*, 137–142. [CrossRef] [PubMed]
18. Chung, C.J.; Long, H.Y. Systematic strontium substitution in hydroxyapatite coatings on titanium via micro-arc treatment and their osteoblast/osteoclast responses. *Acta Biomater.* **2011**, *7*, 4081–4087. [CrossRef] [PubMed]
19. Fang, B.; Wan, Y.Z.; Tang, T.T.; Gao, C.; Dai, K.R. Proliferation and osteoblastic differentiation of human bone marrow stromal cells on hydroxyapatite/bacterial cellulose nanocomposite scaffolds. *Tissue Eng. Part A* **2009**, *15*, 1091–1098. [CrossRef] [PubMed]
20. He, D.; Xiao, X.; Liu, F.; Liu, R. Chondroitin sulfate template-mediated biomimetic synthesis of nano-flake hydroxyapatite. *Appl. Surf. Sci.* **2008**, *255*, 361–364. [CrossRef]
21. Garai, S.; Sinha, A. Biomimetic nanocomposites of carboxymethyl cellulose–hydroxyapatite: Novel three dimensional load bearing bone grafts. *Coll. Surf. B* **2014**, *115*, 182–190. [CrossRef] [PubMed]

22. Cellet, T.P.; Pereira, G.M.; Muniz, E.C.; Silva, R.; Rubira, A.F. Hydroxyapatite nanowhiskers embedded in chondroitin sulfate microspheres as colon targeted drug delivery system. *J. Mater. Chem. B* **2015**, *3*, 6837–6846. [CrossRef]
23. Silva, R.; Pereira, G.M.; Muniz, E.C.; Rubira, A.F. Calcium carbonate crystallization on a polyethylene surface containing ultrathin layers of hydrophilic polymers. *Cryst. Growth Des.* **2009**, *9*, 3307–3312. [CrossRef]
24. Gu, Y.; Huang, J. Ultrathin cellulose film coating of porous alumina membranes for adsorption of superoxide dismutase. *J. Mater. Chem. B* **2013**, *1*, 5636–5643. [CrossRef]
25. Joshi, M.K.; Tiwari, A.P.; Maharjan, B.; Won, K.S.; Kim, H.J.; Park, C.H.; Kim, C.S. Cellulose reinforced nylon-6 nanofibrous membrane: Fabrication strategies, physicochemical characterizations, wicking properties and biomimetic mineralization. *Carbohydr. Polym.* **2016**, *147*, 104–113. [CrossRef] [PubMed]
26. Zhou, C.; Wu, Q.; Yue, Y.; Zhang, Q. Application of rod-shaped cellulose nanocrystals in polyacrylamide hydrogels. *J. Coll. Interface Sci.* **2011**, *353*, 116–123. [CrossRef] [PubMed]
27. Bayol, E.; Gürten, A.A.; Dursun, M.; Kayakırılmaz, K. Adsorption behavior and inhibition corrosion effect of sodium carboxymethyl cellulose on mild steel in acidic medium. *Acta Phys. Chim. Sin.* **2008**, *24*, 2236–2242. [CrossRef]
28. Solomon, M.M.; Umoren, S.A.; Udosoro, I.I.; Udoh, A.P. Inhibitive and adsorption behaviour of carboxymethyl cellulose on mild steel corrosion in sulphuric acid solution. *Corros. Sci.* **2010**, *52*, 1317–1325. [CrossRef]
29. Rajeswari, V.; Kesavan, D.; Gopiraman, M.; Viswanathamurthi, P. Physicochemical studies of glucose, gellan gum, and hydroxypropyl cellulose—Inhibition of cast iron corrosion. *Carbohydr. Polym.* **2013**, *95*, 288–294. [CrossRef] [PubMed]
30. Arukalam, I.O.; Madufor, I.C.; Ogbobe, O.; Oguzie, E.E. Adsorption and inhibitive properties of hydroxypropyl methylcellulose on the acid corrosion of mild steel. *Int. J. Appl. Sci. Eng. Res.* **2013**, *2*, 613–629.
31. Sangeetha, Y.; Meenakshi, S.; Sundaram, C.S. Corrosion inhibition of aminated hydroxyl ethyl cellulose on mild steel in acidic condition. *Carbohydr. Polym.* **2016**, *150*, 13–20. [CrossRef] [PubMed]
32. Liesiene, J.; Kazlauske, J. Functionalization of cellulose: Synthesis of water-soluble cationic cellulose derivatives. *Cellul. Chem. Technol.* **2013**, *47*, 515–525.
33. Cui, W.; Beniash, E.; Gawalt, E.; Xu, Z.; Sfeir, C. Biomimetic coating of magnesium alloy for enhanced corrosion resistance and calcium phosphate deposition. *Acta Biomater.* **2013**, *9*, 8650–8659. [CrossRef] [PubMed]
34. Lin, B.; Zhong, M.; Zheng, C.; Cao, L.; Wang, D.; Wang, L.; Liang, J.; Cao, B. Preparation and characterization of dopamine-induced biomimetic hydroxyapatite coatings on the AZ31 magnesium alloy. *Surf. Coat. Technol.* **2015**, *281*, 82–88. [CrossRef]
35. Bakhsheshi-Rad, H.R.; Hamzah, E.; Kasiri-Asgarani, M.; Jabbarzare, S.; Iqbal, N.; Kadir, M.R. Deposition of nanostructured fluorine-doped hydroxyapatite–polycaprolactone duplex coating to enhance the mechanical properties and corrosion resistance of Mg alloy. *Mater. Sci. Eng. C* **2015**, *60*, 526–537. [CrossRef] [PubMed]
36. Kokubo, T.; Takadama, H. How useful is SBF in predicting in vivo bone bioactivity? *Biomaterials* **2006**, *27*, 2907–2915. [CrossRef] [PubMed]
37. Song, Y.; Han, E.-H.; Shan, D.; Yim, C.D.; You, B.S. The effect of Zn concentration on the corrosion behavior of Mg–*x*Zn alloys. *Corros. Sci.* **2012**, *65*, 322–330. [CrossRef]
38. Fragal, E.H.; Cellet, T.S.; Fragal, V.H.; Companhoni, M.V.; Ueda-Nakamura, T.; Muniz, E.C.; Silva, R.; Rubira, A.F. Hybrid materials for bone tissue engineering from biomimetic growth of hydroxyapatite on cellulose nanowhiskers. *Carbohydr. Polym.* **2016**, *152*, 734–746. [CrossRef] [PubMed]
39. Laurencin, D.; Almora-Barrios, N.; Leeuw, N.H.; Gervais, C.; Bonhomme, C.; Mauri, F.; Chrzanowski, W.; Knowles, J.C.; Newport, R.J.; Wong, A.; et al. Magnesium incorporation into hydroxyapatite. *Biomaterials* **2011**, *32*, 1826–1837. [CrossRef] [PubMed]
40. Bakhsheshi-Rad, H.R.; Hamzah, E.; Daroonparvar, M.; Saud, S.N.; Abdul-Kadir, M.R. Bi-layer nano-TiO_2/FHA composite coatings on Mg–Zn–Ce alloy prepared by combined physical vapour deposition and electrochemical deposition methods. *Vacuum* **2014**, *110*, 127–135. [CrossRef]
41. Jia, X.; Xu, M.; Wang, Y.; Ran, D.; Yang, S.; Zhang, M. Polydopamine-based molecular imprinting on silica-modified magnetic nanoparticles for recognition and separation of bovine hemoglobin. *Analyst* **2013**, *138*, 651–658. [CrossRef] [PubMed]

42. Singh, A. Hydroxyapatite, a biomaterial: Its chemical synthesis, characterization and study of biocompatibility prepared from shell of garden snail, Helix aspersa. *Bull. Mater. Sci.* **2012**, *35*, 1031–1038. [CrossRef]
43. Sureshkumar, M.; Lee, C.K. Polydopamine coated magnetic-chitin (MCT) particles as a new matrix for enzyme immobilization. *Carbohydr. Polym.* **2011**, *84*, 775–780. [CrossRef]
44. Ren, Y.; Zhou, H.; Nabiyouni, M.; Bhaduri, S.B. Rapid coating of AZ31 magnesium alloy with calcium deficient hydroxyapatite using microwave energy. *Mater. Sci. Eng. C* **2015**, *49*, 364–372. [CrossRef] [PubMed]
45. Fekry, A.M.; Ameer, M.A. Corrosion inhibition of mild steel in acidic media using newly synthesized heterocyclic organic molecules. *Int. J. Hydrog. Energy* **2010**, *35*, 7641–7651. [CrossRef]
46. Hu, J.M.; Zhang, J.Q.; Cao, C.N. Determination of water uptake and diffusion of Cl^- ion in epoxy primer on aluminum alloys in NaCl solution by electrochemical impedance spectroscopy. *Prog. Org. Coat.* **2003**, *46*, 273–279. [CrossRef]
47. Fekry, A.M.; El-Sherif, R.M. Electrochemical corrosion behavior of magnesium and titanium alloys in simulated body fluid. *Electrochim. Acta* **2009**, *54*, 7280–7285. [CrossRef]